Molecular Crystals and Liquid Crystals Science and Technology. Section A. Molecular Crystals and Liquid Crystals

Publication details, including instructions for authors and subscription information:
http://www.tandfonline.com/loi/gmcl19

Theory and Simulation of Gas Diffusion in Cholesteric Liquid Crystal Films

Alejandro D. Rey [a]

[a] Department of Chemical Engineering, McGill University, Montreal, Quebec, H3A2A7, Canada

Version of record first published: 04 Oct 2006

To cite this article: Alejandro D. Rey (1997): Theory and Simulation of Gas Diffusion in Cholesteric Liquid Crystal Films, Molecular Crystals and Liquid Crystals Science and Technology. Section A. Molecular Crystals and Liquid Crystals, 293:1, 87-109

To link to this article: http://dx.doi.org/10.1080/10587259708042767

Mol. Cryst. Liq. Cryst., 1997, Vol. 293, pp. 87–109
Reprints available directly from the publisher
Photocopying permitted by license only

Theory and Simulation of Gas Diffusion in Cholesteric Liquid Crystal Films

ALEJANDRO D. REY

Department of Chemical Engineering, McGill University, Montreal, Quebec H3A2A7, Canada

(Received 5 December 1995; In final form 19 August 1996)

Theory and simulation of the dynamical phenomena that characterizes gas diffusion in a cholesteric film are presented. A classical mass transfer theory for cholesteric liquid crystals was used to construct a model that describes the one dimensional transient gas diffusion in a film. The boundary conditions that describe the concentration and orientation conditions in a gas-liquid crystal surface were obtained using the Euler-Lagrange equations for surface reorientations. Numerical solutions to the coupled mass transfer-orientation equations are presented and used to develop a comprehensive view of the phenomena. The main governing parameters that control gas diffusion in a cholesteric film are identified. Two different regimes are identified: (i) diffusion limited regime, and (ii) orientation limited regime. The diffusion limited regime is characterized by strong concentration-orientation couplings, enhanced mass transfer, and up-hill diffusion. The orientation limited regime is characterized by weaker concentration-orientation couplings, and weaker mass transfer enhancements. Conditions that lead to enhanced gas absorption are identified, characterized, and explained in terms of the orientational contribution to the mass flux. Conditions that lead to the uncoiling of the cholesteric helix into a nematic ordering are identified, and the kinetics of the phase transformation is characterized.

Keywords: Gas diffusion; cholesteric liquid crystals; thin films; mass transfer

1. INTRODUCTION

Cholesteric or chiral nematic liquid crystals are an important class of biological and synthetic materials, in which the average macroscopic molecular orientation (director) displays a twist distortion in a direction normal to the molecules, [1,2] known as the cholesteric helix, whose pitch Pe is the

distance required for the director to complete a full 2π rotation. Certain solutions of DNA [3], solutions polypeptides in suitable organic solvents, solutions of hydroxypropylcellulose in water, and cholesterol derivatives are examples of cholesteric liquid crystals [1,2]. A number of potential applications of cholesteric liquid crystals are based on the sensitivity of the cholesteric pitch to pressure, temperature, and concentration [1,2,4]. For example the temperature sensitivity of the cholesteric pitch is a property that allows these materials to be used as temperature sensors. This occurs because cholesterics reflect light whose wave length is equal to the pitch of the helix, thus producing a characteristic color in the presence of white light. Since the characteristic color corresponds to a specific temperature, a color-based temperature scale can be constructed. A similar sensitivity of the cholesteric pitch to organic vapors has been reported some time ago, [4] thus establishing that these materials may be used for detection of organic vapors. Experimental work [4,5] does show that cholesteric liquid crystal films are able to detect certain vapors at even very small concentrations. Thus simulation of diffusion in cholesteric films may be of practical utility in future development of chemical sensors based liquid crystalline materials.

The basis for the ability of cholesterics to be used as concentration sensors rest on phenomena that are essentially similar in thermal sensors [1,6]. Couplings between orientation and temperature gradients or between orientation and concentration gradients arise [1,2,6] because cholesterics liquid crystals do not have mirror symmetry. These macroscopic phenomena are generally known in the presence of free surfaces as the Lehmann effect [1,2,6]. For example a concentration gradient (polar vector) along the cholesteric helix will result in a net torque (axial vector) on the director field, and conversely a twisting of the helix will result in a macroscopic mass flux along the helix. The coupling of mass transfer and orientational order in chiral materials offers new potential applications as chemical sensors, since cholesterics can be incorporated in PDLC (polymer dispersed liquid crystals), cholesteric side-chain liquid crystals, and cholesteric elastomers. We then expect that theory and simulation of concentration gradients-orientation couplings may be useful in developing sensors based on chiral materials.

The objectives of this paper are: (i) to use classical cholesteric constitutive equations to develop a general model that describes the dynamics of one dimensional gas diffusion in cholesteric films, with the helix parallel to the concentration gradient; (ii) to use the model to characterize the basic mass transfer modes in chiral media, and to identify the parameter envelope for

each mode; (iii) to characterize novel effects arising from the mass transfer-orientation coupling, such as gas superabsorbance and untwisting of the cholesteric helix.

The organization of this paper is as follows. Section 2 presents the governing equations, scaling constants, boundary conditions, and defines the cholesteric liquid crystalline order. Section 3 presents the results and discussion. Analysis of the orientation and concentration fields is given, and the main mass transfer-orientation modes are identified. Subsequently, novel phenomena arising from the intrinsic couplings of orientation with concentration gradients in chiral media is given. Section 4 presents the main conclusions of this work.

2. GOVERNING EQUATIONS

2.1. Macroscopic Variables and Geometry

In this section we introduce the macroscopic variables needed to describe the transient 1-D gas diffusion of a solute in a planar (i.e. 2-D orientation) cholesteric film, and define the geometry of the system.

The perfect planar helical ordering characteristic of cholesterics at equilibrium is captured by a unit vector (director) $\mathbf{n}_e(z)$ such that:

$$\mathbf{n}_e(z) = (\cos\theta_e(z), \sin\theta_e(z), 0) \tag{1}$$

where the subscript "e" denotes equilibrium and where the orientation angle at equilibrium $\theta_e(z)$ is given by

$$\theta_e = \frac{2\pi}{P_e} z = \frac{\pi}{p_e} z; \quad P_e = 2p_e \tag{2}$$

where P_e is the equilibrium pitch of the helix, or distance in which the director rotates by 2π radians, and where $p_e = P_e/2$ is the equilibrium half-pitch. The sign of the pitch can be either positive or negative, corresponding to right and left handed helices, respectively. For the present case the axis of the helix is oriented along the z axis.

The concentration of the solute gas in the cholesteric liquid crystal solvent is designated by C (mass/volume), and the equilibrium solubility of the gas in the chiral solvent, at the given temperature and pressure, is designated by C_0. Here we consider isothermal gas diffusion and for a given

cholesteric C_0 is a known constant. The pitch of the cholesteric helix is a function of the gaseous solute concentration [1,2]. For simplicity and without loss of generality we shall assume that concentration dependence of the pitch is given by:

$$P = P_e(1 + \beta' C) \tag{3}$$

such that when $C=0$, $P=P_e$. It will be apparent in what follows that Eqn.(3) only appears as a boundary condition, that is with $P=P_e(1+\beta' C_0)=P(C_0)\equiv$ constant, so that the type of concentration dependence (i.e. linear, non-linear) will not affect the results, since the only relevant quantity is the numerical value $P(C_0)$. If $\beta>0$ ($\beta<0$), the gaseous solute increases (decreases) the pitch. We emphasize that for dilute solutions of optically active media in nematic solvents the resulting cholesteric has a pitch given by PC = constant, [1] but this is not the case studied in this paper; as mentioned above here we study the diffusion of a gaseous solute in a cholesteric solvent.

Consider a planar cholesteric liquid crystal film of thickness L, resting on a solid impermeable boundary suddenly exposed at time $t=0^+$ to a gaseous atmosphere, as shown in Figure 1. For times $t\leqslant 0$ there is no gas present within the film, $C(z,t)=0$. The helix axis is the vertical direction (z-coordinate) and $n_z\equiv 0$. At $z=0$ there is an interface between the cholesteric liquid crystal and a gaseous atmosphere, that contains a soluble solute of equilibrium solubility C_0, and on which the director $\mathbf{n}$ is able to reorient. The use of the equilibrium concentration boundary condition is a classical assumption in diffusion and mass transfer studies [12, 13, 14]. We note that in actual experiments the partial pressure p_0 of the gaseous solute is the controlled variable. Assuming that the classical Henry's law [12, 13, 15] applies, then we find that $p_0 = H\,Co$, where H is the experimentally measured Henry's law constant. Thus knowing H, a given partial pressure p_0 uniquely determines the equilibrium solubility Co, and the adopted boundary condition introduces no unphysical effects or impediments to compare the simulation results with actual experimental data. At $z=L$ there is an impermeable boundary such that the gas flux is zero ($\partial C/\partial z=0$), and on which the director orientation is fixed at a constant angle for all times. Note that the present case corresponds to a concentration gradient always parallel to the cholesteric helix. To describe one dimensional transient gas diffusion in an isothermal incompressible planar cholesteric film of thickness L, in the absence of macroscopic flow and external fields, and under isothermal conditions, we

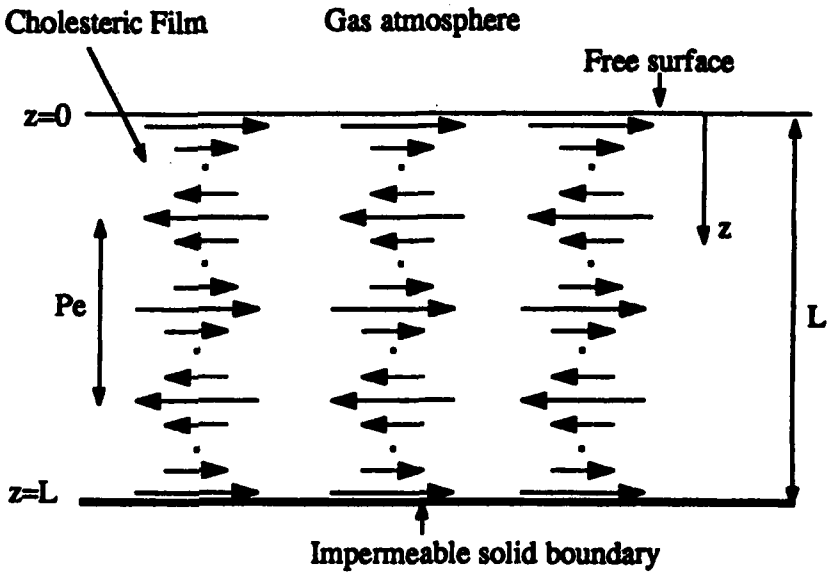

FIGURE 1 Schematic of gas diffusion in a cholesteric film, and definition of the geometry. A planar cholesteric film of thickness L, rests on a solid impemeable boundary suddenly exposed at time $t = 0^+$ to a gaseous atmosphere. For times $t \leqslant 0$ there is no gas present within the film, $C(z, t) = 0$. The helix axis is the z-axis, and $n_z \equiv 0$. At $z = 0$ there is an interface between the cholesteric liquid crystal and a gaseous atmosphere, that contains a soluble solute of equilibrium solubility C_0, and on which the director $\mathbf{n}$ is able to reorient. At $z = L$ there is an impermeable boundary, and the director orientation is fixed. Concentration gradients ($\partial C/\partial z$) are coupled to orientation changes ($\partial\theta/\partial t$).

then must specify the following orientation and concentration fields:

$$\mathbf{n} = \mathbf{n}(z, t),\ C = C(z, t),\ \mathbf{n}.\mathbf{n} = 1,\ C \geqslant 0,\ t > 0,\ 0 \leqslant z \leqslant L \tag{4}$$

where constraints appear in both dependent variables.

2.2. Governing Equations, Auxiliary Conditions, and Scaling

The balance equations for gas diffusion in a cholesteric liquid crystal film are the torque balance equation and the mass balance equation [1],

$$\Gamma^e + \Gamma^v = 0 \tag{5a}$$

$$\frac{\partial C}{\partial t} = -\nabla.\mathbf{J} \tag{5b}$$

where Γ^e is the elastic torque per unit volume and Γ^v is the viscous torque per unit volume acting on the director, and where $\mathbf{J}$ is the mass flux vector (mass/area time). The constitutive equation for the elastic torque Γ^e is given by [1]:

$$\Gamma^e = \mathbf{n} \times \mathbf{h}^e \equiv -\mathbf{n} \times \left[\frac{\partial F}{\partial \mathbf{n}} - \nabla . \frac{\partial F}{\partial \nabla_{\mathbf{n}}} \right] \tag{6}$$

where $\mathbf{h}^e$ is the elastic molecular field and F is the free energy density, given by [1]:

$$2F = K_{11}(\nabla . \mathbf{n})^2 + K_{22}(\mathbf{n} . \nabla \times \mathbf{n})^2 + K_{33}|\mathbf{n} \times \nabla \times \mathbf{n}|^2 \tag{7}$$

where the $\{K_{ii}\}$ are the Frank elastic moduli for splay, twist, and bend, respectively [1]. In this work the Frank moduli are considered to be given constants. In the absence of macroscopic flow, the constitutive equation for the viscous torque Γ^v is given by [1]:

$$\Gamma^e = -\mathbf{n} \times \mathbf{h}^v \equiv -\mathbf{n} \times \left[\gamma_1 \frac{\partial \mathbf{n}}{\partial t} + \nu \alpha \, \mathbf{n} \times \nabla C \right] \tag{8}$$

where $\mathbf{h}^v$ is the viscous molecular field, γ_1 is the rotational viscosity, ν is a coupling reactive parameter, and α is the proportionality constant between the chemical potential gradient $\nabla \mu$ and the concentration gradient ∇C, $\nabla \mu = \alpha \nabla C$, and where μ is the chemical potential per unit mass. Note that a concentration gradient normal to the director results in an elastic torque. In the absence of macroscopic flow the constitutive equation for the mass flux is given by [1]:

$$\mathbf{J} = -\left[D_\perp \nabla C + (D_{//} - D_\perp) \left(\mathbf{n} . \nabla C \right) \mathbf{n} + \nu \mathbf{n} \times \frac{\partial \mathbf{n}}{\partial t} \right] \tag{9}$$

where $D_\perp (D_{//})$ is the diffusivity normal (along) the director. Note that orientation transients in a cholesteric liquid crystal solvent give rise to a solute mass flux.

With the adopted planar 1-D planar director field $(\mathbf{n}(z,t) = (n_x(z,t), n_y(z,t), 0))$, and 1-D concentration field $(C = C(z,t))$, the equations (1, 5, 6, 8, 9) that govern the dynamics of the solute concentration $C(z,t)$ and the director orientation $\theta(z,t)$ simplify to the following coupled linear partial differential equations:

$$\frac{\partial C}{\partial t} = D_{\perp}\frac{\partial^2 C}{\partial z^2} + \nu\frac{\partial}{\partial z}\left(\frac{\partial \theta}{\partial t}\right) \tag{10a}$$

$$\gamma_1\frac{\partial \theta}{\partial t} = K_{22}\frac{\partial^2 \theta}{\partial z^2} + \nu\alpha\frac{\partial C}{\partial z} \tag{10b}$$

The units of the physical parameters appearing in the governing bulk equations are as follows: $D_{\perp}$(length^2/time), ν(viscosity × time/length), γ_1(viscosity), K_{22}(energy/length), α (length^2/(concentration × time^2)).

The required auxiliary conditions are two initial conditions and four boundary conditions. The initial conditions describing the sudden contact of the gaseous solute on a pure planar cholesterol at equilibrium is given by:

$$t = 0, \quad 0 \leqslant z \leqslant L, \quad C = 0, \quad \mathbf{n} = \mathbf{n}_e \tag{11}$$

where for simplicity we set $L = N \times P_e$, and where N is the number of pitches contained in the film of thickness L in the absence of the solute ($C = 0$, $0 \leqslant z \leqslant L$).

The solute boundary condition at the gas-liquid crystal interface is:

$$z = 0, \quad t > 0, \quad C = C_0 \tag{12}$$

which assumes equilibrium at all times. The concentration boundary condition at the liquid crystal-solid boundary at $z = L$ is given by:

$$t > 0, \quad J_z|_{z=0} = -D_{\perp}\left.\frac{\partial C}{\partial z}\right|_{z=0} = 0 \tag{13a}$$

$$z = 0, \quad t > 0, \quad \frac{\partial C}{\partial z} = 0 \tag{13b}$$

which describes an impermeable surface and the presence of fixed director orientation.

At steady state, the adopted director orientation at the gas-liquid crystal interface is dictated by the free surface (i.e. zero torque) conditions. Since the solute concentration changes the pitch of the cholesteric liquid crystal, the differential equation that governs the director reorientation at the gas-liquid

crystal boundary is given by the Euler-Lagrange equation for surface motion [7]. The Euler-Lagrange equation for surface motion for the present case is given by the following balance between dissipation and elastic storage:

$$z=0, \quad \frac{\partial R^s}{\partial \dot{\theta}}+\Phi_\theta=0 \tag{14}$$

where a superpose dot denoted time differentiation, R^s is the Rayleigh dissipation function, and Φ_θ is the generalized elastic force. Assuming a linear frictional force $\partial R^s/\partial\dot{\theta}$ we find [7] the following expression for the dissipation function R^s:

$$R^s=\frac{\lambda^s}{2}\dot{\theta}^2 \tag{15}$$

where λ^s is a surface viscosity, a subscript denotes partial differentiation. The frictional force acting on the director due to orientational slip is

$$\frac{\partial R^s}{\partial \dot{\theta}}=\lambda^s\dot{\theta} \tag{16}$$

The elastic force is obtained from the surface contribution to the variation of the total elastic free energy of the system. For the present geometry, the total free energy Λ, neglecting kinetic energy and surface energy contributions, in a volume V of cholesteric liquid crystal is:

$$\Lambda=\int_v F(\theta,\theta_z)\,dV; \quad F=\frac{K_{22}}{2}\left(\frac{\partial\theta}{\partial z}-q\right)^2, \quad q(C)=\frac{2\pi}{P} \tag{17a,b,c}$$

$q(C)$ denotes the wave vector ($q=2\pi/P$) corresponding to the concentration C. The variation of Λ is

$$\delta\Lambda=\int_v\left[\frac{\partial F}{\partial\theta}\delta\theta+\frac{\partial F}{\partial\theta_z}\delta\theta_z\right]dV \tag{18}$$

Using the Gauss theorem, $\delta\Lambda$ becomes

$$\delta\Lambda=\int_v\left[\frac{\partial F}{\partial\theta}-\frac{\partial}{\partial z}\frac{\partial F}{\partial\theta_z}\right]\delta\theta\,dV+\int_s\frac{\partial F}{\partial\theta_z}\zeta_z\delta\theta\,dS \tag{19}$$

where ζ is the outward unit normal to the enclosing surface S of the volume V. The generalized elastic force Φ_θ due to bulk deformations at the gas-liquid crystal surface located at $z=0$ is

$$\Phi_\theta = \frac{\partial F}{\partial \theta_z}\zeta_z = -\frac{\partial F}{\partial \theta_z} = -K_{22}\frac{\partial \theta}{\partial z} \tag{20}$$

where the minus sign in front of K_{22} takes into account the direction of the outward unit normal to the gas-liquid crystal interface. Introducing the explicit dependence of the pitch on concentration (eqn. (3) evaluated at $z=0$), and substituting (16, 18) into (14), the equation for surface reorientation becomes:

$$\lambda^s \frac{\partial \theta}{\partial t} = K_{22}\left(\frac{\partial \theta}{\partial z} - \frac{2\pi}{P_e(1+\beta' C_0)}\right) \tag{21}$$

At steady state ($\partial\theta/\partial t = 0$), or if the surface viscosity is neglected ($\lambda^s \equiv 0$), we recover the classical [1] free surface boundary condition: $\partial\theta/\partial z = q$. The orientation boundary condition at $z=L$ is fixed at: $\theta(z=L, t>0) = 2\pi L/P_e$.

Next we introduce the time and length scales of the model. The length scales of the model are the equilibrium pitch $P_e(C=0)$, the pitch $P(C_0)$, and the macroscopic film thickness $L = NP_e$. The five extrinsic (i.e. L dependent) time scales of the model are:

$$\tau_0 = \frac{\gamma_1 L^2}{K_{22}}; \quad \tau_D = \frac{L^2}{D_\perp}; \quad \tau_c^1 = \frac{\gamma_1 L}{\alpha|v|C_0}; \quad \tau_c^2 = \frac{\gamma_1 C_0 L^3}{|v|K_{22}}; \quad \tau_s = \frac{\lambda^s L}{K_{22}} \tag{22}$$

where τ_0 is the orientation relaxation time, τ_D is the mass diffusion relaxation time, τ_c^1 and τ_c^2 are the coupled diffusion-orientation relaxation times appearing in (10b) and (10a), respectively. Replacing L by P_e in (2) we obtain the five intrinsic time scales. The intrinsic length and time scales describe local intra-pitch variations and the extrinsic scales describe the macroscopic slower changes. In (20) we use the magnitude $|v|$ since the sign of the reactive coupling is undetermined. The four time scales ratios used below are:

$$r_1 = \frac{\tau_0}{\tau_D}; \quad r_2 = \frac{\tau_0}{\tau_c^2}; \quad r_3 = \frac{\tau_0}{\tau_c^1}; \quad B = \frac{\tau^s}{\tau_0} \tag{23}$$

As usual the non-negative entropy production imposes restrictions on the signs of certain parameters, as discussed in [1], and for the present model we require that $\gamma_1 \geqslant 0$ and $D_\perp \geqslant 0$. Recalling that the pitch varies with concentration according (3), it follows that to satisfy the non-negative definite concentration constraint ($C \geqslant 0$) the following restriction must hold:

$$\text{sign}(\beta') = -\text{sign}(v) \tag{24}$$

which follows from (10a). For example, if a gas decreases the cholesteric pitch ($\beta' < 0$) and v is assumed to be negative, unphysical negative concentration are found. Equation (24) on the other hand will result always in physically meaningful positive solute concentrations.

Non-dimensionalizing the governing equations and boundary conditions using L as a length scale, C_0 as a concentration scale, and τ_0 as a time scale, the model equations and auxiliary conditions become:

$$\frac{\partial C^*}{\partial t^*} = r_1 \frac{\partial^2 C^*}{\partial z^{*2}} - \text{sign}(\beta') r_2 \frac{\partial}{\partial z^*}\left(\frac{\partial C^*}{\partial t^*}\right); \quad t^* > 0, \quad 0 \leqslant z^* \leqslant 1 \tag{25a}$$

$$\frac{\partial \theta}{\partial t^*} = \frac{\partial^2 \theta}{\partial z^{*2}} - \text{sign}(\beta') r_3 \frac{\partial C^*}{\partial z^*}; \quad t^* > 0, \quad 0 \leqslant z^* \leqslant 1 \tag{25b}$$

$$t^* = 0, \quad 0 \leqslant z^* \leqslant 1, \quad C^* = 0 \tag{25c}$$

$$t^* = 0, \quad 0 \leqslant z^* \leqslant 1, \quad \theta = 2\pi N z^* \tag{25d}$$

$$t^* > 0, \quad z^* = 0, \quad C^* = 1 \tag{25e}$$

$$t^* > 0, \quad z^* = 0, \quad \frac{\partial \theta}{\partial z^*} = B \frac{\partial \theta}{\partial t^*} + \frac{2\pi}{1+\beta}; \quad \beta = \beta' C_0 \tag{25f}$$

$$t^* > 0, \quad z^* = 1, \quad \frac{\partial C^*}{\partial z^*} = 0 \tag{25g}$$

$$t^* > 0, \quad z^* = 1, \quad \theta = 2\pi N \tag{25h}$$

where $C^* = C/C_0$, $z^* = z/L$, and $t^* = t/\tau_0$.

The six parameters of the model are: r_1, r_2, r_3, β, B, and N. Without loss of generality in this paper we set $N=5$ and $B=0.001$, thus assuming that the bulk reorientation is much slower than at the gas-liquid crystal interface. In this paper we assume equal coupling constants ($r_2=r_3=1$), and investigate the effects of β and r_1 on the coupled orientation-diffusion response. The variation of β captures the effect of pitch variation on the orientation-diffusion response, and the variation of r_1 captures the effect of the diffusion to orientation time constant ratio on the orientation-diffusion response:

$$r_1=\frac{\tau_0}{\tau_D}=\frac{\gamma_1 D_\perp}{K_{22}} \tag{26}$$

The two limiting behaviors arising from variations in r_1 are:

(i) Diffusion limited response (DLR), $r_1<1$

Materials with fast reorientation (small γ_1), such as low molar mass cholesterics, may operate under DLR. Although no complete data seems to be available, using reported diffusivity and viscoelastic data for PAA (a low molar mass nematic) [1,8] we find: $D_\perp \approx 3\times 10^{-6}\,\text{cm}^2/\text{sec}$; $K_{22}=4.3\times 10^{-7}$ dynes; $\gamma_1=0.067$ poise, and the ratio of the orientation relaxation time to the diffusion time is less than on, $r_1=0.467<1$.

(ii) Orientation limited response (OLR), $r_1>1$

Materials with slow reorientation times (larger γ_1), such as cholesteric polymers, are expected operate under OLR. No complete set of transport coefficients is yet available for cholesteric polymers. Using an estimate of the diffusion coefficient of a polymer liquid crystal [9], we find $D_\perp \approx 2\times 10^{-7}\,\text{cm}^2/\text{sec}$. Estimates of viscoelastic parameters for nematic polymers [10] are: $K_{22}=0.6\times 10^{-7}$ dynes; $\gamma_1=139$ poise, and the resulting estimated ratio of the orientation relaxation time to the diffusion time is much greater than one, $r_1=463\gg 1$.

For simplicity and efficiency, the governing equations (22) are integrated numerically using Galerkin Finite Elements (GFEM) [11] with 20 linear elements to discretize the spatial terms, and an implicit corrector-predictor Euler method with adaptive time step to dicretize the time dependent terms. The advantage of this hybrid method is that the boundary condition (22f), itself a differential equation, is easily handled when using GFEM in conjunction with integration by parts [11].

3. RESULTS AND DISCUSSION

In this section we present and discuss the solutions to (25), that describe the transient orientation-diffusion response of a cholesteric film suddenly placed in contact with a soluble gas. We characterize three basic phenomena: (i) the dynamics of the transient orientation-diffusion response, (ii) the film absorbance properties, and (iii) the kinetics of diffusion-induced phase transitions, including the cholesteric→ nematic transition and the nematic→ cholesteric transition.

3.1. Dynamics of Diffusion-Orientation Response

A. Diffusion Limited Response (DLR): $r_1 < 1$

This regime is characterized by the following ordering in the time relaxation constants:

$$\tau_0 = \tau_c^1 = \tau_c^2 < \tau_D \tag{27}$$

and the relaxation time for uncoupled mass transfer τ_D is larger than the relaxation time for uncoupled reorientations τ_0. Since diffusion drives the orientation relaxation process, the reorientation and diffusion relaxation are strongly coupled. The strongly coupled system will achieve steady state when $t^* \approx \tau_D$.

Figure 2 shows the dimensionless concentration C^* (top) and the director orientation θ (bottom) as a function of the dimensionless distance z^*, for four increasing times, $r_1 = 0.1$ and $\beta = 1$. The dimensionless times t^* are: 0.0012 (dashed line), 1.88 (dashed dot line), 10 (dashed triple dot line), and steady state (full line). In both graphs the full line denotes steady state. The arrows in the top graph indicates the direction of change of the particular profile. At early times (dashed line) the concentration develops a peak that eventually leads to a monotonically increasing profile, whose maximum is larger than one ($C^*\text{max} > 1$). At later times the profile evolves towards the homogeneous steady state $C^* = 1$. Mass diffusion is singularly characterized by an early localized pulse, by up-hill diffusion (mass transfer from low concentration to high concentration), and by the presence of solute concentrations larger than the solubility C_0. The bottom graph indicates that for $\beta = 1$ the pitch increases homogeneously, and that in the intermediate stage (dashed dot line) nonlinearities are weak. The graph shows that $\theta(z^* = 0, t \to \infty) = 5\pi$, in agreement with (3) when $\beta = 1$.

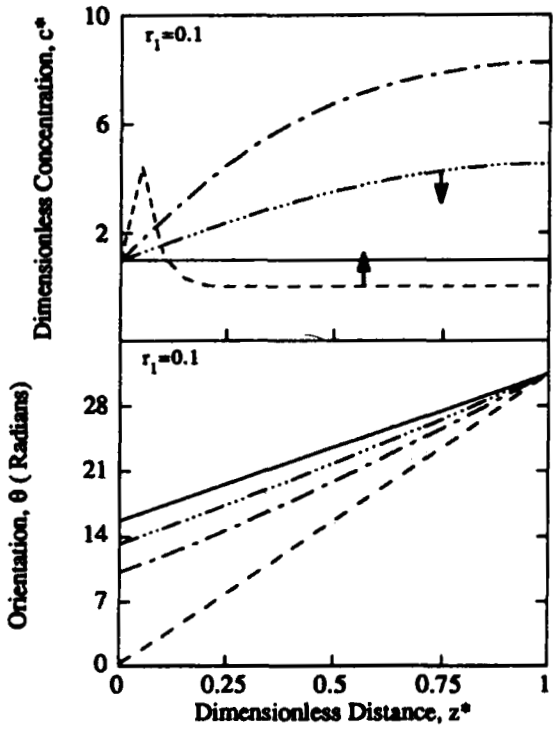

FIGURE 2 Dimensionless concentration C^* (top) and the director orientation θ (botton) as a function of the dimensionless distance z^*, for four increasing times, $r_1 = 0.1$ and $\beta = 1$. The dimensionless times t^* are: 0.0012 (dashed line), 1.88 (dashed dot line), 10 (dahsed triple dot line), and steady state (full line). In both graphs the full line denotes steady state. The arrows in the top graph indicates the direction of change of the particular profile. At early times (dashed line) the concentration develops a peak that eventually leads to a monotonically increasing profile, whose maximum is larger than one ($C^*\max > 1$). At later times the profile evolves towards the homogeneous steady state $C^* = 1$. The bottom graph indicates that for $\beta = 1$ the pitch increases homogeneously.

Figure 3 shows the dimensionless concentration C^* (top) and the director orientation θ (bottom) as a function of the dimensionless distance z^*, for four increasing times (same as in Fig. 2), $r_1 = 0.1$ and $\beta = -0.5$. In both graphs the full line denotes steady state. The arrows in the top graph indicates the direction of change of the particular profile. Mass diffusion is again characterized by an early localized pulse, by up-hill diffusion, and by the presence of solute concentrations larger than the solubility C_0, except that the coupling orientation now produces a much more enhanced solute absorption (compare the top graphs of Figs. (2–3) and note the different scales). The effect arises from the coupling term $\partial(\partial\theta/\partial t^*)/\partial z^*$ which has an

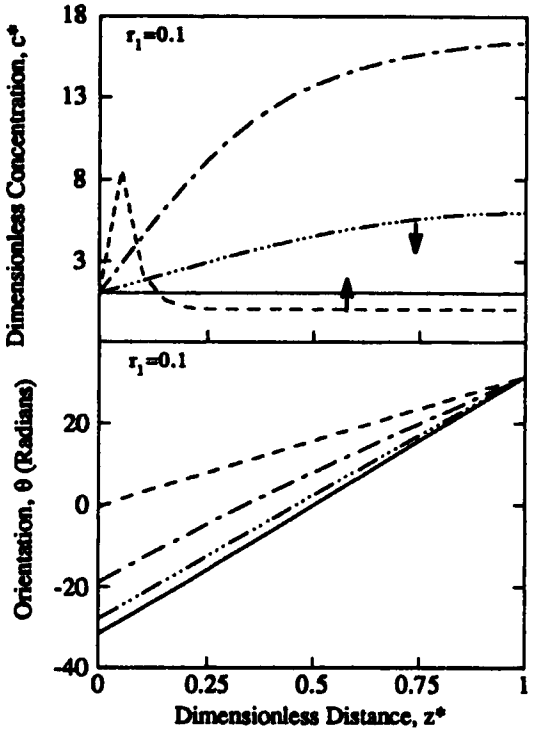

FIGURE 3 Dimensionless concentration C^* (top) and the director orientation θ (bottom) as a function of the dimensionless distance z^*, for four increasing times (same as in Fig. 2), $r_1 = 0.1$ and $\beta = -0.5$. In both graphs the full line denotes steady state. The arrows in the top graph indicates the direction of change of the particular profile. Mass diffusion is again characterized by an early localized pulse, by up-hill diffusion, and by the presence of solute concentrations larger than the solubility C_0, except that the coupling orientation now produces a much more enhanced solute absorption (compare the top graphs of Figs. (2–3) and note the different scales).

initial magnitude increase in the present case ($\beta = -0.5$) but decreases monotonically to zero in the $\beta = 1$ case. The evolution of the orientation is now characterized by a decrease in the cholesteric pitch. For $\beta = -0.5$ the graph shows that $\theta(z^* = 0, t \to \infty) = -5\pi$, in agreement with (3).

As $r_1 \to 0$ the overall system response becomes infinitely slow and the mass transfer into the film is governed by the coupling term r_2. In such limiting case the orientation also slows down since it is an enslaved variable due to the coupling term introduced by r_3. Figure 4 shows the dimensionless concentration C^* (top) and the director orientation θ (bottom) as a function of the dimensionless distance z^*, for four increasing times, $r_1 = 0.001$ and $\beta = 1$. The dimensionless times t^* are: 0.00321 (dashed line),

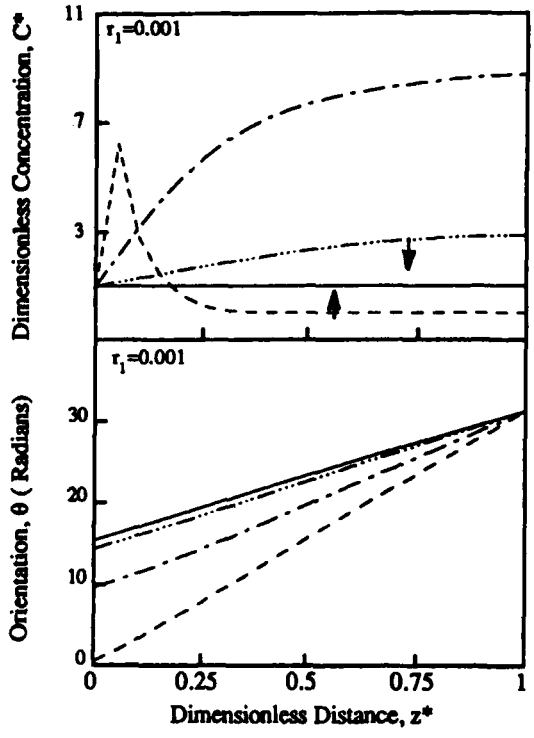

FIGURE 4 Dimensionless concentration C^* (top) and the director orientation θ (bottom) as a function of the dimensionless distance z^*, for four increasing times, $r_1 = 0.001$ and $\beta = 1$. The dimensionless times t^* are: 0.00321 (dashed line), 95 (dashed dot line), 1868 (dashed triple dot line), and steady state (full line). In this limiting regime the kinetics of the response is dominated by the coupling terms and the steady state is essentially achieved at $t^* \approx 1/r_1 = 1000$.

95 (dashed dot line), 1868 (dashed triple dot line), and steady state (full line). In this limiting regime the kinetics of the response is dominated by the coupling terms and the steady state is essentially achieved at $t^* \approx 1/r_1 = 1000$.

B. Orientation Limited Response (OLR) : $r_1 > 1$

This regime is characterized by the following ordering in the time relaxation constants:

$$\tau_0 = \tau_c^1 = \tau_c^2 > \tau_D \tag{28}$$

and the relaxation time for uncoupled mass transfer τ_D is smaller than the relaxation time for uncoupled reorientations τ_0. It is instructive to briefly consider the limiting behavior of this regime which occurs when $r_1 = \varepsilon \gg 1$. For very fast diffusion and slow reorientation, the concentration quickly achieves a steady state $C^* = 1$ when $t^* \approx 1/\varepsilon$, and the concentration and orientation fields decoupled. The orientation field evolves towards the steady state unaffected by the concentration, and the term introduced by r_3 in Eqn. (22b) is negligible since $C^* \approx 1$ and $\partial C^*/\partial z^* \approx 0$. Assuming for simplicity that $\lambda^s = 0$ and after the fast initial transient die out ($t^* > 1/\varepsilon$), the solution to the governing equations (22) when $r_1 = \varepsilon \gg 1$, are given by

$$C^* = 1 \tag{29a}$$

$$\theta(z^*, t^*) = \left[\frac{2\pi N}{1+\beta}(z+\beta)\right] - \frac{2\pi N\beta}{1+\beta}\sum_{n=1}^{\infty}\frac{8}{(2n-1)^2\pi^2}\exp\left\{-\left[(2n-2)\frac{\pi}{2}\right]^2 t^*\right\}\cos(2n-1)\frac{\pi}{2}z^* \tag{29b}$$

The time scales for the orientation relaxation towards the linear steady state profile $\theta = 2\pi N(z^* + \beta)/(1 + \beta)$ are:

$$\tau_{0,n} = \frac{4}{(2n-1)^2\pi^2}\left(\frac{\gamma_1 L^2}{K_{22}}\right); \quad n = 1, 2, 3, \ldots \tag{30}$$

which shows that the longest relaxation time is $4\,\tau_0/\pi^2$.

Figure 5 shows the dimensionless concentration C^* (top) and the director orientation θ (bottom) as a function of the dimensionless distance z^*, for four increasing times, $r_1 = 10$ and $\beta = 1$. The dimensionless times t^* are: 0.001 (dahsed line), 0.08 (dahsed dot line), 0.47 (dashed triple dot line), and steady state (full line). In both graphs the full line denotes steady state. The arrows in the top graph indicates the direction of change of the particular profile. The concentration does not develop a localized pulse at early stage, and the maximum absorbance is weaker than for $r_1 = 0.1$. The pitch decreases virtually homogeneously as in Figure 2. For $r_1 > 1$, the diffusion

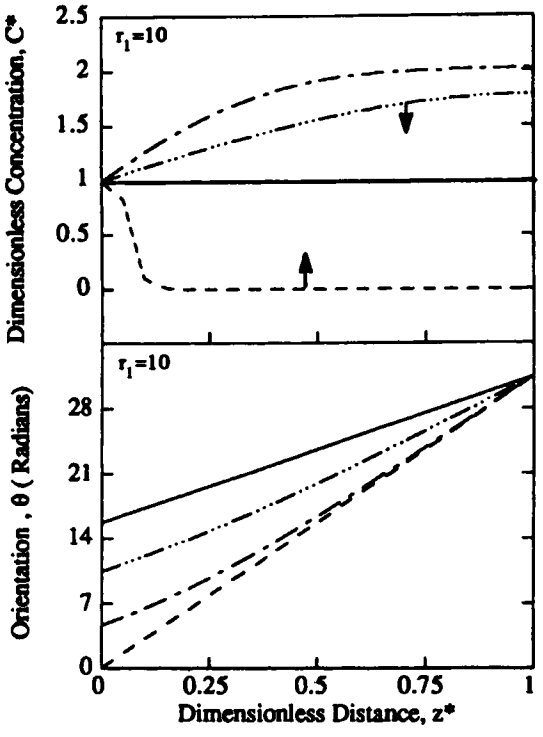

FIGURE 5 Dimensionless concentration C^* (top) and the director orientation θ (bottom) as a function of the dimensionless distance z^*, for four increasing times, $r_1 = 10$ and $\beta = 1$. The dimensionless times t^* are: 0.001 (dashed line), 0.08 (dashed dot line), 0.47 (dashed triple dot line), and steady state (full line). In both graphs the full line denotes steady state. The arrows in the top graph indicates the direction of change of the particular profile. The concentration does not develop a localized pulse at early stage, and the maximum absorbance is weaker than for $r_1 = 0.1$. The pitch decreases virtually homogeneously as in Figure 2. For $r_1 > 1$, the diffusion term tends to weaken the absorption effect from the time dependent orientation gradients. The steady state is reached at a dimensionless time $t^* \approx 1$, which is the slowest relative scale.

term tends to weaken the absorption effect from the time dependent orientation gradients. The steady state is reached at a dimensionless time $t^* \approx 1$, which is the slowest relative scale. Comparing Figures 2 and 5 (same $\beta = 1$) the main differences in the transient responses are the absence of a localized pulse at early stage, and the maximum absorbance for $r_1 = 10$ is weaker than for $r_1 = 0.1$.

Figure 6 shows the dimensionless concentration C^* (top) and the director orientation θ (bottom) as a function of the dimensionless distance z^*, for four increasing times, $R_1 = 10$ and $\beta = -0.5$. The dimensionless times t^* are: 0.001 (dashed line), 0.092 (dashed dot line), 0.568 (dashed triple dot line),

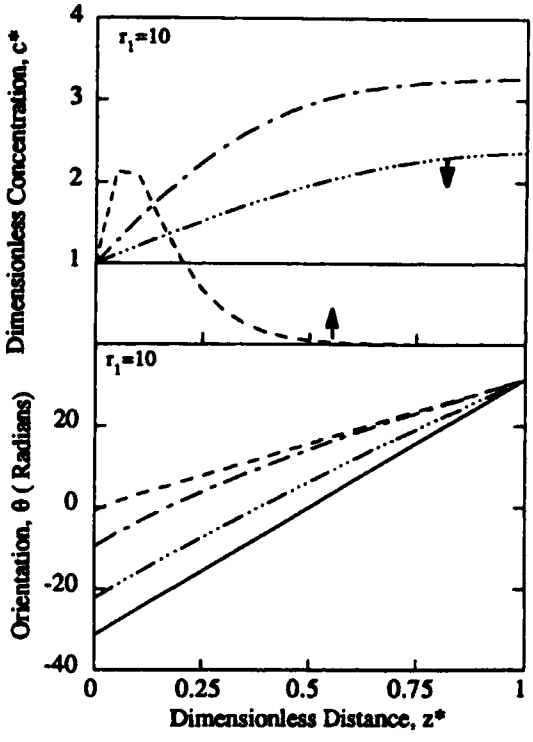

FIGURE 6 Dimensionless concentration C^* (top) and the director orientation θ (bottom) as a function of the dimensionless distance z^*, for four increasing times, $R_1 = 10$ and $\beta = -0.5$. The dimensionless times t^* are: 0.001 (dashed line), 0.092 (dashed dot line), 0.568 (dashed triple dot line), and steady state (full line). The concentration pulse is now again present since the orientation effect is stronger but the pulse is broader since diffusion is now stronger. Steady state is reached in one dimensionless time unit. The maximum concentration is lower than for the $r_1 < 1$ case.

and steady state (full line). The concentration pulse is now again present since the orientation effect is stronger but the pulse is broader since diffusion is now stronger. Steady state is reached as in one dimensionless time unit. The maximum concentration is lower than for the $r_1 < 1$ case.

As mentioned above, as $r_1 \to \infty$ the mass transfer into the film is independent of the coupling term r_2. In this limiting regime mass transfer occurs by diffusion and is uncoupled to orientation. The concentration profile evolves as in an isotropic fluid with a time constant dictated by $1/r_1$. In addition no initial concentration pulse forms, and up-hill diffusion is not present.

In partial summary, the mechanisms that govern the transient phenomena that characterizes the gas diffusion in cholesteric films have been identified. In

the presence of non-negligible couplings ($r_1 < 1$) the response is strongly affected by whether the gas increases or decreases the cholesteric pitch and on the relative ratio of orientation to concentration relaxation times. Unique transient mass transfer features, favored in the orientation limited regime and also for gases that decrease the pitch, are increased gas absorption above the solubility limit and up-hill diffusion. For the studied cases the orientation profiles exhibit weak non-linearities.

3.2. Film Absorbance Properties

In this section we briefly discuss the absorbance properties of the cholesteric film. The main characteristic of the absorbance is the maximum amount of solute dissolved in the film. In the absence of mass transfer-orientation couplings the maximum absorbed amount per unit area is just $C_0 \times L$. In the presence of mass transfer-orientation couplings it has been shown above that a great enhancement in absorbance is present, in particular if the solute decreases the pitch. According to Eqn. (9) the mass flux in the z direction is given by:

$$J_z = J_z^d + J_z^0, \quad J_z^d = -D_\perp \frac{\partial C}{\partial z}, \quad J_z^0 = \nu \frac{\partial \theta}{\partial t} \tag{31}$$

where J_z^d is the mass flux due to diffusion and J_z^0 is the mass flux due to temporal orientation changes. Gases that greatly affect the pitch will exhibit superabsorbance, since J_z^0 will be greatly enhanced. To characterize this effects we introduce the following time dependent scaled maximum absorbed mass M^* per unit area:

$$m^*(t) = \frac{m(t)}{C_0 L} = \int_0^1 C^* \, dz^*, \quad \max\{m^*\} = M^* \tag{32}$$

where M^* is the maximum value attained by m^*. To find M^*, we numerically integrate the concentration profile using a three point Gaussian quadrature [11], construct a time series, and pick the largest value.

Figure 7 shows the scaled maximum absorbed mass M^* as a function of the solute power β, for $N = 5$, and for r_1:0.1 (full line), 1 (dashed dot line), and 10 (dashed triple dot line). To the right (left) of the vertical line the pitch increases (decreases). The figure shows that for gases that decrease the pitch

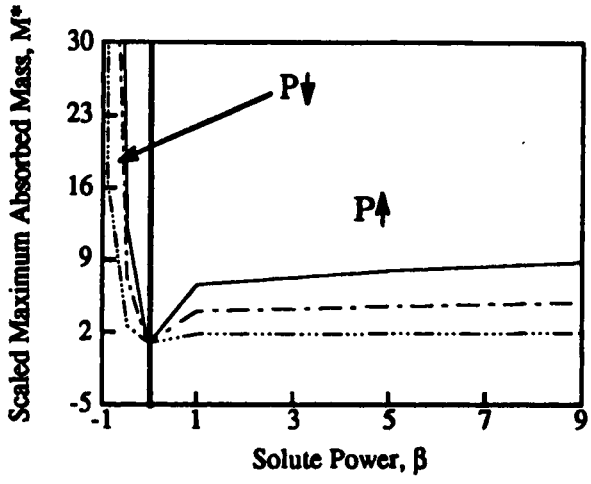

FIGURE 7 Scaled maximum absorbed mass M^* as a function of the solute power β, for $N = 5$, and for r_1:0.1 (full line), 1 (dashed dot line), and 10 (dashed triple dot line). To the right (left) of the vertical line the pitch increases (decreases). The figure shows that for gases that decrease the pitch ($\beta < 0$) absorption is greatly enhanced and that for gases that decrease the pitch ($\beta > 0$) absorption is weakly enhanced. In the limiting case that $\beta \to -1$, super absorption occurs due to the orientation-induced mass flux.

($\beta < 0$) absorption is greatly enhanced and that for gases that decrease the pitch ($\beta > 0$) absorption is weakly enhanced. In the limiting case that $\beta \to -1$, superabsorption occurs due to the orientation-induced mass flux.

3.3. Kinetics of Phase Transitions

In this section we discuss the kinetic of phase transitions that may occur when a solute untwists the cholesteric helix resulting in the cholesteric→nematic transition ($C \to N$). The objective is to characterize this novel mass transfer induced phase transition in a constrained thin film geometry. Although in actual cases the concentration dependence of the pitch may not follow Eqn. (3), the predictions shown here capture the basic features of the phenomena. To simulate the $C \to N$ transition we note that in the present model the parameter that controls the steady state pitch is β, here called the solute power. Thus, to capture the $C \to N$ transition we compute the limiting behavior as $\beta \to \infty$, which according to Eqn. (3) predicts that the pitch diverges: $P \to \infty$. To avoid redundant information we only show the time evolution of the director surface orientation, $\theta(z^* = 0, t^* > 0)$, since the concentration and orientation profiles are similar to those discussed in detail above.

Figure 8 shows the director surface orientation, $\theta(z^* = 0)$ as a function of dimensionless time. The values of r_1 are: 0.1 (full line), 1 (dashed dot line), and 10 (dashed triple dot line). The parameter values are: $N = 5$, and $\beta = 10^6$. For the chosen values the initial linear cholesteric orientation profile is given by: $\theta(z^*) = 10\pi z^*$. The final nematic orientation state is attained when the constant orientation is $\theta = 10\pi$ everywhere, including the surface at $z^* = 0$. The figure shows that all the curves start from zero (cholesteric) and eventually reach a value of 10π (nematic). The figure shows that increasing r_1 increases the rate of phase transformation. The $C \rightarrow N$ transition is characterized by exponential growth (decay) with multiple time constants. For large r_1 a good approximation to the surface orientation $\theta(z^* = 0, t^* > 0)$ is:

$$\theta(z^* = 0, t^*) = 2\pi N - 2\pi N \sum_{n=1}^{\infty} \frac{8}{(2n-1)^2\pi^2} \exp\left\{-\left[(2n-2)\frac{\pi}{2}\right]^2 t^*\right\} \quad (33)$$

which shows the presence of multiple relaxation times, as found numerically.

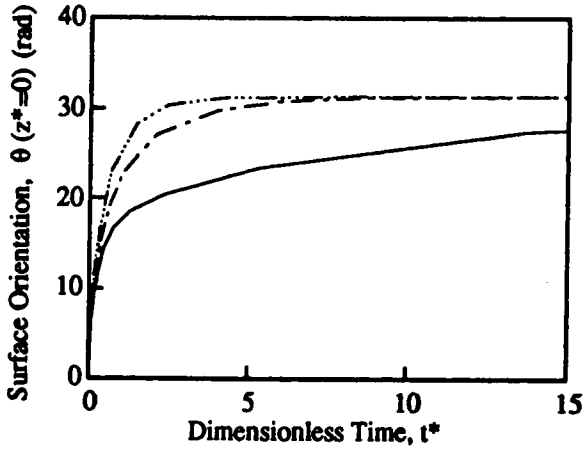

FIGURE 8 Director surface orientation, $\theta(z^* = 0)$ as a function of dimensionless time. The values of r_1 are: 0.1 (full line), 1 (dashed dot line), and 10 (dashed triple dot line). The parameter values are: $N = 5$, and $\beta = 10^6$. The figure shows that all the curves start from zero (cholesteric) and eventually reach a value of 10π (nematic). The figure shows that increasing r_1 increases the rate of phase transformation. The $C \rightarrow N$ transition is characterized by exponential growth with multiple time constants.

4. CONCLUSIONS

A classical mass transfer theory for cholesteric liquid crystals was used to simulate one dimensional transient gas diffusion in a cholesteric film. Analysis of the concentration and orientation dynamics indicates that mass transfer in cholesteric liquid crystal films may follow two different regimes. If diffusion is slower than reorientation the response is diffusion limited, and if orientation is slower than diffusion the response is orientation limited. Cholesteric polymers are very likely to follow the latter mode due to large rotational viscosities, while low molar mass cholesterics may follow the former mode since reorientation is fast. The diffusion limited regime is characterized by strong concentration-orientation couplings, enhanced mass transfer, and up-hill diffusion. The orientation limited regime is characterized by weaker concentration-orientation couplings, and weaker mass transfer enhancements. Conditions that lead to enhanced gas absorption are identified, characterized, and explained in terms of the orientational contribution to the mass flux. Conditions that lead to the uncoiling of the cholesteric helix into a nematic ordering are identified, and the kinetics of the phase transformation is characterized.

The theory and simulation presented here provide certain guidelines that may be useful in optimizing the use of cholesteric films as organic vapor sensors. These guidelines include the relevant physical parameters and the unique dynamical phenomena that arise due to the orientation-concentration couplings. The conditions that lead to superabsorbance may also be of interest in fundamental studies of supersaturation.

Acknowledgements

This work is supported by the Natural Science and Engineering Research Council of Canada. The author is thankful to the McGill University Computing Center for a grant to defray the computational costs of this research.

References

[1] P. G. de Gennes and J. Prost, "The Physics of Liquid Crystals", 2nd edition (Clarendon Press, Oxford, 1993).
[2] S. Chandrasekhar, "Liquid Crystals", 2nd edition (Cambridge University Press, Cambridge, 1992).
[3] A. Leforestier and F. Livolant, *J. Phys. II France 2*, 1853 (1992).
[4] J. L. Fergason, *Scientific America*, **211**, 77 (1964).

[5] E. J. Poziomek, T. J. Novak and R. A. Mackay, *Mol. Cryst. Liq. Cryst.*, **27**, 175 (1974).
[6] H. R. Brand, *Phys. Rev. A*, **37**, 2736 (1988).
[7] A. D. Rey, Periodic textures of Nematic Polymers and Orientational Slip, *Macromolecules*, **24**, 4450–4456 (1991).
[8] P. K. Khabibullaev, E. V. Gevorkyan and A. S. Lagunov, "Rheology of Liquid Crystals", Allerton Press Inc, New York, 1994.
[9] H. Hakemi, *J. Polym. Science: Polymer Letters Edition*, **24**, 377 (1986).
[10] S. D. Lee and R. B. Meyer, in Liquid Crystallinity in Polymers, A. Cifferri ed., VCH Publishers, Inc, New York, p. 357, 1991.
[11] B. A. Finlayson, "Nonlinear Analysis in Chemical Engineering", McGraw-Hill, New York, p. 28, 1980.
[12] W. R. Vieth, "Diffusion In and Through Polymers", Hanser Publishers, Munich, p. 19, 1991.
[13] E. L. Cussler, "Diffusion", Cambridge University Press, New York, p. 36, 1984.
[14] G. W. Castellan, Physical Chemistry 3rd edition, Addison-Wesley Publishing Company, Reading, Massachusetts, p. 312, 1983.
[15] R. B. Bird, W. E. Stewart and E. N. Lightfoot, "Transport Phenomena", John Wiley & Sons, New York, p. 519, 1960.